CIRP Annals - Manufacturing Technology 63 (2014) 553–556

Contents lists available at ScienceDirect

CIRP Annals - Manufacturing Technology

journal homepage: http://ees.elsevier.com/cirp/default.asp

Generation of hierarchical micro-structures for anisotropic wetting by elliptical vibration cutting

Ping Guo [a], Yong Lu [b], Kornel F. Ehmann [a], Jian Cao (2)[a,*]

[a] Department of Mechanical Engineering, Northwestern University, Evanston, IL 60208, USA
[b] State Key Laboratory of Automotive Safety and Energy, Tsinghua University, Beijing, China

ARTICLE INFO

Keywords:
Surface modification
Micro machining
Anisotropic wetting

ABSTRACT

This paper reports enhanced anisotropic wettability using two-level hierarchical micro-structures. First-order micro-channels with superimposed second-order micro-textures were machined on aluminum surfaces using ultrasonic elliptical vibration cutting (EVC). Controllable sinusoidal micro-textures with a wavelength one order of magnitude smaller than the widths of the first-order micro-channels were applied to the surface. Anisotropic wettability was evaluated by water contact angle measurements in two orthogonal directions. The results have shown that the generated hierarchical micro-structures have nearly doubled the anisotropic contact angle in comparison to one-level structures. A relationship between anisotropic wetting characteristics and process parameters is also presented.

1. Introduction

Research on engineered surfaces for manipulating surface wettability has attracted much interest in both industry and academia due to its potential applications in high performance micro-fluidic devices, self-cleaning surfaces, biomedical products, etc. [1]. Surface wettability is often characterized by the water contact angle (CA). For an isotropic surface, the water droplet tends to remain of a spherical shape due to its minimal energy state, in which no particular direction is favored. Researchers have found that asymmetric designs of surface structures introduce anisotropic wettability [2], in which the water droplet contact angles are different depending on the direction in which the angle is measured. For example, in the case of parallel channels, apparent contact angles are measured in directions parallel and perpendicular to the channels and denoted as $\theta_{||}$ and $\theta_{\perp}$, as shown in Fig. 1. The water droplet tends to elongate in the channel direction, forming an ellipsoid, and thus yielding a smaller contact angle, $\theta_{||}$, compared to the perpendicular contact angle, $\theta_{\perp}$. The difference between these two angles, $\Delta\theta$, is a representative quantity that characterizes the anisotropic wettability of the surface [3].

Anisotropic wetting is observed in nature on many biological surfaces. Their hierarchical structures are one of the key factors to achieve high anisotropic wetting. For example, the hierarchical micro-structures on rice leafs induce strong anisotropic wetting to encourage water droplets to slide along the longitudinal direction of the leaf [4]. Another example is the surface of butterfly wings. The hierarchical arrangement of micro-scales and nano-stripes facilitates the water droplets to roll off the wings [5]. The hierarchical structures of these two examples are shown in Fig. 2.

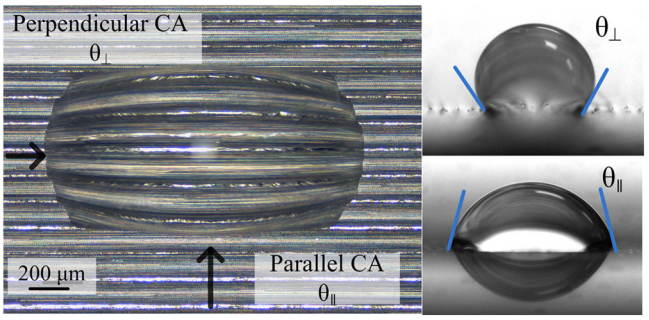

Fig. 1. Anisotropic droplet and contact angle definition.

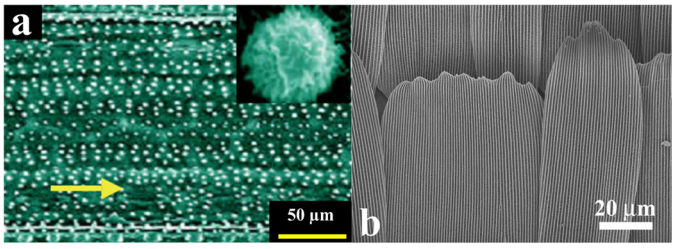

Fig. 2. SEM images of (a) rice leaf [4] and (b) butterfly wing [6].

Inspired by nature, researchers have been exploring different fabrication techniques to efficiently produce artificial hierarchical structures for enhanced anisotropic wetting. Nanoimprint lithography was used to sequentially pattern two-order structures on

* Corresponding author.

http://dx.doi.org/10.1016/j.cirp.2014.03.048
0007-8506/© 2014 CIRP.

polystyrene (PS) and PMMA films [7]. Since metal surfaces are of specific interest for many industrial applications, femtosecond laser ablation has been reported to create periodic surface structures on stainless steel surfaces [8]. However, the existing methods are still limited in terms of their mass production capability due to high cost, long processing times, and material restrictions.

This paper proposes a vibration-assisted machining method, inspired by elliptical vibration cutting (EVC), to generate hierarchical micro-structures on metal surfaces in a one-step machining process. It is based, as described in Section 2, on the overlapping of elliptical tool trajectories to generate controlled second-order textures, while machining the first-order micro-channels. Micro-channels with and without second-order textures have been generated on aluminum surfaces as described in Section 3. Their anisotropic wettability was measured and reported in Section 4 showing strong anisotropic wettability. A linear relationship has been found between the anisotropic angle and the channel gap distance.

2. Elliptical vibration cutting

The original idea of EVC to utilize largely overlapping elliptical trajectories for improved cutting performance was proposed by Moriwaki and Shamoto [9]. The principle of the EVC process is shown in Fig. 3. The cutting tool usually vibrates along an elliptical trajectory in the cutting plane at an ultrasonic frequency. The tool vibration, when coupled with a slow feed motion (i.e., smaller than the maximal vibration velocity in the cutting direction), results in overlapping tool trajectories. This brings two-fold benefits to the cutting operation: (1) the reverse motion of the tool turns the continuous cutting into an intermittent process, which reduces the average cutting forces and increases tool life; (2) the overlapping tool trajectories reduce the effective chip thickness, which facilitates a ductile-mode cutting regime when machining brittle materials [10]. The machined surfaces are left with periodic marks due to the overlapping trajectories. The frequency and wavelength of these cusps, or micro-textures, are determined by the vibration amplitudes as well as the nominal feed velocity. In conventional EVC processes, the feed velocity is often kept very small, so that the process can even produce a much better surface finish than that produced by traditional machining, e.g., a nano-metric surface finish. Since the actual cutting period during each cycle is also decreasing with the decrease of the nominal feed velocity, the instantaneous uncut chip thickness is dramatically reduced.

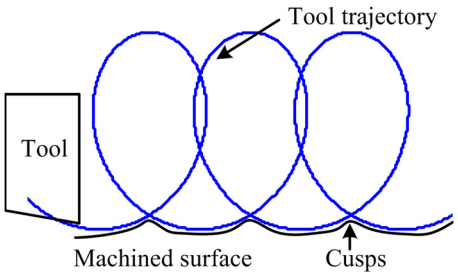

Fig. 3. Schematic of elliptical vibration cutting.

The proposed method, although also termed EVC, unlike conventional EVC uses very high feed velocities that result in loosely packed tool trajectories for surface texture generation. Here, vibration-induced micro-textures are utilized to generate hierarchical structures in a one-step machining process. The first-order micro-channels (on the order of tens to a few hundred microns) are generated by applying elliptical vibrations in a grooving operation. The second-order textures (on the order of a tenth to a few microns) are simultaneously created due to the overlapping tool trajectories in consecutive vibration cycles. The nominal feed velocity in this case is then determined according to the required wavelength of the second-order micro-textures.

The tool trajectory can be decomposed into two sinusoidal functions in the cutting and depth-of-cut directions with a linear feed motion in the cutting direction, which can be expressed by:

$$\begin{aligned} x &= A\sin(\omega t) + vt \\ y &= B\sin(\omega t) + \varphi \end{aligned} \tag{1}$$

where x and y are tool positions in the cutting and depth-of-cut directions; A and B are the vibration amplitudes; ω is the tool vibration angular velocity; φ is the displacement phase angle between the two vibrations; and v is the nominal feed velocity.

Given a fixed tool vibration frequency, the wavelength of the micro-textures is determined by the relative tool motion in the cutting direction during a full vibration cycle, i.e.,

$$\lambda = \frac{2\pi v}{\omega} \tag{2}$$

The coordinates of the cusps in the cutting plane satisfy the following set of equations:

$$\begin{aligned} &A\cos\left(\frac{\theta_1+\theta_2}{2}\right)\sin\left(\frac{\theta_1-\theta_2}{2}\right) + \frac{v}{\omega}\left(\frac{\theta_1-\theta_2}{2}\right) = 0 \\ &\sin(\theta_1+\varphi) = \sin(\theta_2+\varphi) \end{aligned} \tag{3}$$

where θ_1 and θ_2 are two particular angular positions corresponding to the cusp, with values limited between 0 and 2π. Their particular values can be solved numerically.

The amplitude of the textures in the depth direction is determined by the height of the cusps, i.e., given by:

$$h = B(1 - |\sin(\theta_1 + \varphi)|) \tag{4}$$

3. Experiment and measurement procedures

The EVC principle has been previously applied by the authors for the fast generation of micro-structured surfaces on cylindrical surfaces in the turning operation [11]. A tertiary motion generator (TMG) has been designed to deliver the required ultrasonic elliptical vibrations [12]. The device consists of two Langevin piezoelectric transducers and utilizes their coupled resonant modes in two orthogonal directions to produce amplified elliptical vibrations at the tool tip.

The same TMG has been utilized in this work and adapted to a planer configuration, as shown in Fig. 4. The customized motion stage provides the feed motion in the cutting direction (X-axis) and sets the depth-of-cut (Y-axis) and the cross feed (Z-axis). It is composed of two side wedges and a center wedge. The two side wedges move in the X-axis direction to control the cutting motion, and their relative motion determines the Z-axis motion [13]. An independent Y-axis slide is installed on the center wedge. The stage is controlled by a Delta–Tau UMAC system through a Labview interface.

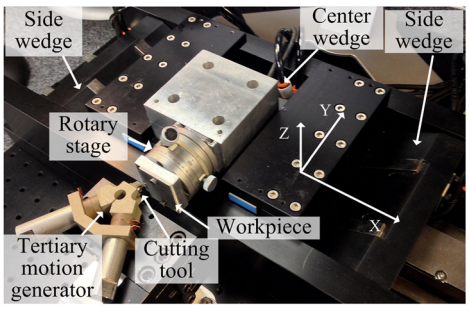

Fig. 4. Experimental setup.

A calibration procedure for the TMG is necessary prior to the experiment. The shape and direction of the vibration trajectory are influenced by the frequency of the sinusoidal excitation signals to the two transducers and the phase shift angle between them. The excitation frequency was adjusted to match the coupled resonant frequency; and the phase shift angle was tuned to control the orientation and direction of the elliptical trajectory. The vibrations

were monitored using two capacitance displacement sensors from MicroSense, which have a sub-nanometer resolution and a 100 kHz bandwidth. The sinusoidal excitation signals were generated by a National Instrument data acquisition card (NI DAQ PCIe-6361) and sampled at 1.5 MHz. The signals were then amplified through a piezo amplifier (TREK PZD 350). The displacement signals from the capacitance sensors were recorded using the same data acquisition card at 500 kHz. The excitation frequency was determined to be 28 kHz, while the phase shift between the two input signals was adjusted to be 95°. These settings achieve the optimal tool trajectory shown in Fig. 5. The tool vibration direction along with its stationary orientation is also illustrated in the figure.

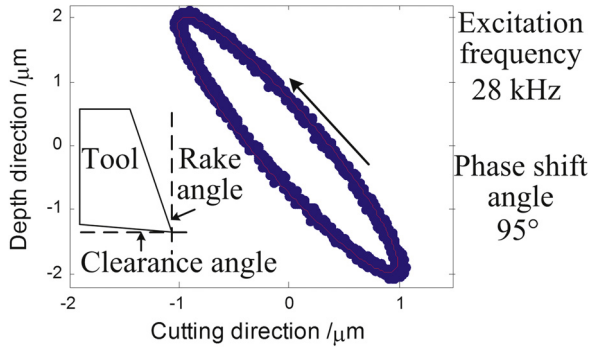

Fig. 5. Recorded tool trajectory.

The cutting tool used to create micro-channels was a commercial polycrystalline diamond (PCD) insert, with a 100 μm nose radius. The rake and clearance angles were 10° and 7°, respectively. Another single-crystal diamond insert with a 500 μm nose radius, 0° rake angle and 7° clearance angle was used to pre-machine the surface. It was used to shape the sample surface without applied vibrations to provide a smooth and flat base for channel generation. The workpiece material used was aluminum alloy AA6061-T4.

The machining procedures are described as follows. The *X*-axis motion provides the feed motion in the cutting direction at a speed of 150 mm/s. When operating without vibrations, the cutting motion was solely provided by the motion stage with a cutting velocity equal to the stage velocity (150 mm/s); while in the EVC mode, the cutting motion is contributed by the combination of the tool vibrations and the feed motion. The workpiece was first machined using the 500 μm insert, with a 50 μm cross feed in the *Z*-axis. The relatively high surface roughness *Ra* of the pre-machined surface of 150 nm, measured in the cutting direction, is attributed to the low cutting speed used. Then, a series of channels were generated using the 100 μm insert. For each sample, a different channel gap was set. For comparison, 8 samples were machined with ultrasonic elliptical vibrations for 8 different channel gaps; while another 8 samples were machined directly without vibration for the same set of channel gaps. The nominal cutting depth was kept constant at 20 μm; however, due to the nose radius of the cutting insert, when the gap is small, the channels start to overlap in the cross feed direction, causing a reduced depth. The actual measured channel gaps and depths are summarized in Fig. 6 for channels generated with and without the elliptical vibrations. It should be noted that one important parameter is constant for all samples, which is the curvature of the channel cross-section profile. It is determined by the tool nose radius (100 μm).

All machined samples were washed using an ultrasonic cleaner and dried under room temperature. The wettability tests were performed using a water contact angle measuring instrument (Krüss GmbH, DSA25). The droplet size was controlled at 1 μL. According to the definition in the introduction part, perpendicular and parallel contact angles (namely, $\theta_{\perp}$ and $\theta_{\parallel}$) were both measured. Each measurement was repeated three times at different locations.

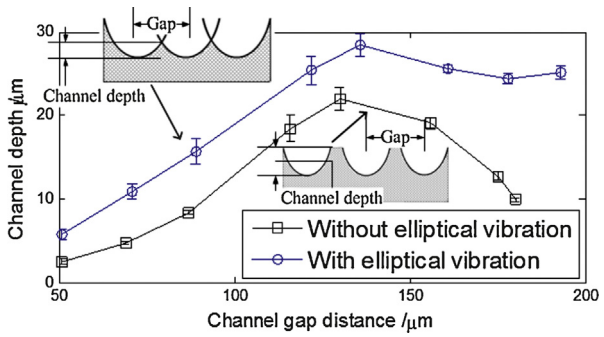

Fig. 6. Measured channel depth for each experiment.

4. Results and discussion

Examples of machined surfaces are given in Fig. 7. Channels machined without and with elliptical vibrations are shown in Fig. 7a and c, respectively. Their appearances allow for making an easy distinction, given their different light reflections. The smooth channels appear to be more reflective and have a glossy finish. The textured channels show a matte finish. Fig. 7b and d shows the magnified views of two different kinds of channels. It can be noticed that vibration-induced textures are distributed over the whole channel surface where the tool contacted the workpiece. Vibration-induced hierarchical structures are demonstrated in Fig. 8. The surface profile, of the first-order structure parallel channel in the cross feed direction is plotted in Fig. 8a. Burr formation was found on one side of the channel wall. The surface profile in the cutting direction at the bottom of the channel is plotted in Fig. 8b. It shows the second-order micro-textures with an amplitude of around 0.5 μm. The wavelength of the textures was calculated from the autocorrelation function of the surface profile to be 5.5 μm, while the theoretical value based on Eq. (2) is 5.4 μm.

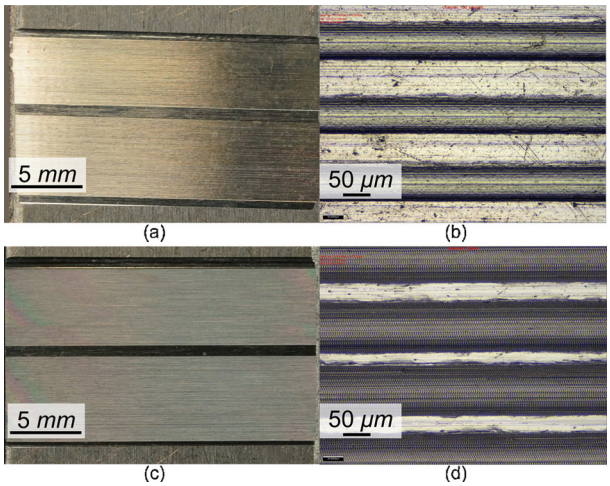

Fig. 7. Machined samples without elliptical vibrations: (a) optical image and (b) magnified view; machined samples with elliptical vibrations: (c) optical image and (d) magnified view.

The measured contact angles in two directions for different channel gap distances are plotted in Fig. 9 for the smooth and textured cases. Due to the anisotropic wettability induced by the micro-channels, the water droplet spreads easier along the channel direction, while it is pinned along the perpendicular direction, as shown in Fig. 1. This confirms the results that the perpendicular contact angles are always larger than the parallel ones, as shown in Fig. 9. For reference, the isotropic contact angle for the flat surface was measured to be $63 \pm 3°$, which is comparable to all the measured $\theta_{\parallel}$. This indicates that hydrophobicity along the channel direction slightly increases, while anisotropic wetting is mainly induced by the increased perpendicular contact angles.

The above results are better interpreted by looking at the anisotropic angle, $\Delta\theta$, defined as the difference between the two

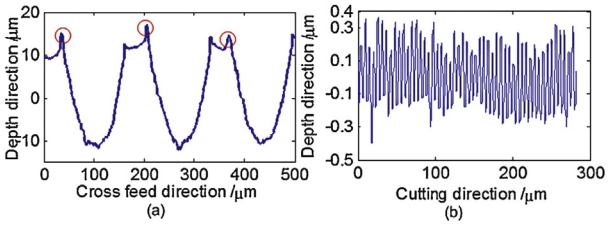

Fig. 8. Surface profiles of the machined sample with elliptical vibrations in (a) the cross feed direction and (b) the cutting direction.

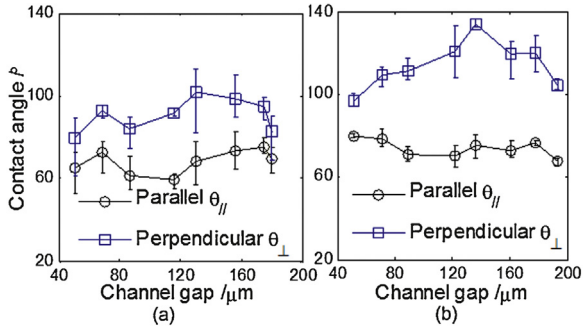

Fig. 9. Contact angles for (a) smooth and (b) textured channels.

measured contact angles. As shown in Fig. 10, it can be seen that anisotropy increases at first with an increase in the channel gap, and then decreases when the gap is further increased. There is a transition point for both textured and smooth channels at which anisotropic wettability is the largest. This can be explained by the simultaneous interaction of two competing mechanisms: (1) the increased channel gap elevates the energy barrier for water to spread perpendicular to the channel, thus enhances anisotropic wetting; and (2) the increased channel gap decreases the number of channels covered by the water droplet, and thus reduces the anisotropic effect.

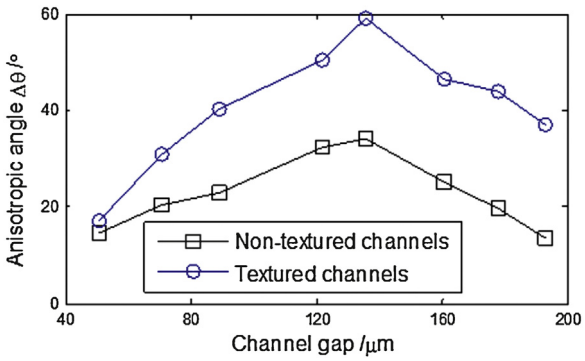

Fig. 10. Anisotropic angle comparison between one-level and hierarchical structures.

The hierarchical structures associated with the textured channels increase overall anisotropic wetting compared to one-level structures. This is further analyzed in Fig. 11, where only the first five increasing data points in Fig. 10 are considered. By a linear regression, the anisotropic angle fits well to a straight line for both textured and smooth channels. The slope of the curve measures the anisotropic wettability induced by the channels. From the figure, it can be seen that the slope for the hierarchical structures is double that for one-level structures (0.4618 vs. 0.2327). In other words this means that the anisotropic angles for textured channels are always twice the values of those for smooth channels. This anisotropy slope indicates an intrinsic property of the surface, which does not depend on the channel gap and is insensitive to channel depth. The intercept of the fitted line in theory should be 0°, where the channels are reduced to a flat surface. The results (+3.09° and −3.78°) match our assumption. The reason for

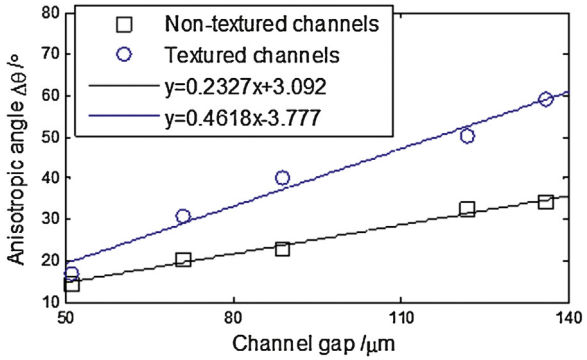

Fig. 11. Linear fit curve for the anisotropic angle.

enhanced anisotropic wetting in hierarchical structures is the composite contact induced by the micro-textures, where air is trapped at the water–solid contact interface.

5. Summary

This paper applies elliptical vibration cutting to the generation of hierarchical micro-structures in a one-step machining process. Inspired by nature, hierarchical structures have been applied to create artificial super-hydrophobic surfaces. It is experimentally verified in this paper, that hierarchical structures also significantly enhance anisotropic wetting in surfaces with parallel channels. It has also been discovered that the anisotropic angle linearly increases with an increase in channel gap for both textured and smooth channels. Future work will include a theoretical framework of surface geometry on anisotropy, and a study on material type, tool geometry and cutting conditions.

Acknowledgements

Financial support from the National Science Foundation under grant number CMMI-0825722 is greatly appreciated. The second author is also grateful for the financial support from the National Natural Science Foundation of China (Grant #51176082).

References

[1] Malshe A, Rajurkar K, Samant A, Hansen HN, Bapat S, Jiang W (2013) Bio-Inspired Functional Surfaces for Advanced Applications. *CIRP Annals – Manufacturing Technology* 62(2):607–628.
[2] Tawfick S, De Volder M, Copic D, Park SJ, Oliver CR, Polsen ES, Roberts MJ, Hart AJ (2012) Engineering of Micro-and Nanostructured Surfaces with Anisotropic Geometries and Properties. *Advanced Materials* 24(13):1628–1674.
[3] Xia D, Johnson LM, López GP (2012) Anisotropic Wetting Surfaces with One-Dimensional and Directional Structures: Fabrication Approaches, Wetting Properties and Potential Applications. *Advanced Materials* 24(10):1287–1302.
[4] Feng L, Li S, Li Y, Li H, Zhang L, Zhai J, Song Y, Liu B, Jiang L, Zhu D (2002) Super-Hydrophobic Surfaces: From Natural to Artificial. *Advanced Materials* 14(24):1857–1860.
[5] Zheng Y, Gao X, Jiang L (2007) Directional Adhesion of Superhydrophobic Butterfly Wings. *Soft Matter* 3(2):178–182.
[6] Dechkrong P, Jiwajinda S, Dokchan P, Kongtungmon M, Chomsaeng N, Chairuangsri T, Yu C-C, Hsiao C-N, Shiojiri M (2011) Fine Structure of Wing Scales of Butterflies, *Euploea mulciber* and *Troides aeacus*. *Journal of Structural Biology* 176(1):75–82.
[7] Zhang F, Low HY (2007) Anisotropic Wettability on Imprinted Hierarchical Structures. *Langmuir* 23(14):7793–7798.
[8] Wu B, Zhou M, Li J, Ye X, Li G, Cai L (2009) Superhydrophobic Surfaces Fabricated by Microstructuring of Stainless Steel Using a Femtosecond Laser. *Applied Surface Science* 256(1):61–66.
[9] Moriwaki T, Shamoto E (1995) Ultrasonic Elliptical Vibration Cutting. *CIRP Annals – Manufacturing Technology* 44(1):31–34.
[10] Nath C, Rahman M, Neo KS (2011) Modeling of the Effect of Machining Parameters on Maximum Thickness of Cut in Ultrasonic Elliptical Vibration Cutting. *Journal of Manufacturing Science and Engineering* 133(1):011007.
[11] Guo P, Ehmann KF (2013) An Analysis of the Surface Generation Mechanics of the Elliptical Vibration Texturing Process. *International Journal of Machine Tools and Manufacture* 64:85–95.
[12] Guo P, Ehmann KF (2013) Development of a Tertiary Motion Generator for Elliptical Vibration Texturing. *Precision Engineering* 37(2):364–371.
[13] Khim G, Ro SK, Park JK, Ehmann K (2012) A Three-Axis Translation Stage Using Opposing Wedges with Error Compensation. *International Journal of Precision Engineering and Manufacturing* 13(3):401–406.